Archive of SID.ir

University of Tehran Press

Journal of the Earth and Space Physics

Homepage: https://jesphys.ut.ac.ir

Vol. 49, No. 4, Winter 2024, P. 105- 119

(Research Article)

Stress Field Inversion Analysis of Earthquake Focal Mechanisms in Northwestern Iran: Implications for Tectonic Regimes

Salmanian, M.[1] | Rastbood, A.[2] ✉ | Mashhadi Hossainali, M.[1]

1. Department of Geodesy, Faculty of Geodesy and Geomatics Engineering, K. N. Toosi University of Technology, Tehran, Iran.
2. Department of Surveying, Faculty of Civil Engineering, University of Tabriz, Tabriz, Iran.

Corresponding Author E-mail: arastbood@tabrizu.ac.ir

(Received: 26 Aug 2023, Revised: 22 Nov 2023, Accepted: 9 Jan 2024, Published online: 20 Feb 2024)

Abstract

Understanding the stress field is crucial for assessing seismic risks in Northwestern Iran, a region known for its high seismic activity and geological volatility. The intricate tectonic arrangements involving the Arabian, Anatolian and Eurasian plates contribute to the unstable nature of the area. This study focuses on deducing stress regimes through stress inversion analysis of earthquake focal mechanisms in the North Tabriz Fault system. Analyzing the stress field is essential for understanding the elastic characteristics and geodynamics of the region. This study considers the stress field surrounding the Tabriz Fault, aiming to determine stress parameters and principal stress orientations using focal mechanisms. By analyzing 35 earthquake focal mechanism datasets from the Global Centered Moment Tensor and the Iranian Seismological Center, stress field inversions were conducted using Michael's linear inversion method and the iterative joint inversion method. The two techniques yielded distinct outcomes, with the iterative joint inversion method proving more accurate in determining stress fields and principal stress orientations. The Plunge values of σ_1 and σ_3 were observed to be relatively insignificant, measuring 3.24 and 2.06, respectively. A value close to 90 degrees, specifically 86.14, was determined for σ_2. The trend values for σ_1 and σ_3 were found to be 146.08 and 55.97, respectively, while σ_2 exhibited a trend value of 293.51. To estimate the orientation of the maximum horizontal stress (SH), the iterative joint inversion method was employed, yielding an estimation of $\alpha = 3.787°$. The trend and plunge calculated from this method for σ_1, σ_2 and σ_3 were also utilized in this estimation. The findings indicate the existence of strike-slip faults in proximity to the North Tabriz Fault. The stress direction observed and the trajectory of the fault system suggest the influence of a transpressional mechanism. The predominant right-lateral strike-slip motion observed aligns with the prevailing tectonic regime in the region, providing evidence of strike-slip and thrust faulting stress regimes. The results contribute to a better understanding of the stress field and geodynamic situation in Northwestern Iran. They provide valuable insights for spatial analysis of future earthquakes and assessing seismic hazards in the region.

Keywords: Stress filed, Focal mechanism, Stress inversion, Horizontal stress (SH), North Tabriz Fault (NTF).

1. Introduction

The northward motion of the Arabian plate has influenced the deformation of the youthful crust in northwestern Iran. Since the Late Miocene, this movement has generated compressive forces along the north-south axis and tensile forces along the east-west axis, resulting in the regulation of volcano distribution and the predominance of strike-slip faults in this region. At the boundary of the Eocene–Oligocene, the collision of the Arabian plate and Eurasia is the determining factor in the regulation of active deformation in Iran (McKenzie, 1972; Jackson and McKenzie, 1984; Dewey et al., 1986; Hempton, 1987; Allen et al., 2004; Agard et al.; 2011; Mouthereau et al., 2012). An investigation into the stress state within the crust has the potential to enhance the comprehension of existing deformation within specific regions, notably the northwest of Iran, due to its intricate seismotectonic conditions. Various techniques have been suggested for ascertaining tectonic stress based on focal mechanisms of earthquakes

Cite this article: Salmanian, M., Rastbood, A., & Mashhadi Hossainali, M. (2024). Stress Field Inversion Analysis of Earthquake Focal Mechanisms in Northwestern Iran: Implications for Tectonic Regimes. *Journal of the Earth and Space Physics*, 49(4), 105- 119. DOI: http//doi.org/10.22059/jesphys.2024.364173.1007555

E-mail: (1) miladsalmaniyan.science@gmail.com | hossainali@kntu.ac.ir

Publisher: University of Tehran Press.
DOI: http//doi.org/10.22059/jesphys.2024.364173.1007555

Print ISSN: 2538-371X
Online ISSN: 2538-3906

Archive of SID.ir

Archive of SID.ir

(Maury et al., 2013). Prevalent techniques have been formulated by Michael (1984), Gephart and Forsyth (1984) and Jacques (2002), which have undergone modifications and enhancements suggested by Lund and Slunga (1999), Hardebeck and Michael (2006), Arnold and Townend (2007), Maury et al. (2013), and other researchers have proposed modifications and expansions to these techniques.

The investigation conducted by Zamani (2013) aimed to examine the stress state existing within the Siahcheshme-Khoy fault zone. The Zamani study revealed that the region under investigation was predominantly subjected to a tectonic stress regime with strike-slip movement. The average stress ratio was determined to be 0.41 for the regional average stress tensor. This outcome was in keeping with prior research conducted by McKenzie (1972), where two sets of conjugate reverse and strike-slip faults were identified in the eastern regions of Turkey and the Caucasus.

Furthermore, the research conducted by Zarifi et al. (2014) utilized the focal mechanisms of crustal earthquakes spanning from 1909 to 2012, along with GPS velocities gathered between 1999 and 2011, in order to estimate the magnitude and orientations of the highest principal stress and strain rates within Iran. The iterative joint inversion method was employed by Afra et al. (2017) to determine the trend/plunge values for σ_1, σ_2 and $\sigma_3$in the northwestern region of Iran. The resulting values were 142/2 for σ_1, 238/73 for σ_2, and 51/17 for σ_3. In the northwest region of Iran, utilizing the multiple inversion method, Afra et al. (2017) acquired the trend/plunge values of 134/1 and 44/5 for σ_1 and σ_3, respectively. Moreover, the stress ratio was determined to be 0.28. Niassarifard et al. (2021) conducted an assessment of trend and plunge values for σ_1, σ_2 and σ_3 in the northwestern area of Iran in accordance with his recently proposed new tectonic configuration. The obtained measurements were 195/00, 55/90 and 285/00, respectively. Aflaki et al. (2021) conducted an examination of the trend and plunge values in the northwestern area of Iran for σ_1, σ_2 and σ_3. The results indicated that the approximate values were 78/00, 326/89 and 168/01, respectively. An analysis of the trend and plunge values in the northwestern region of Iran was carried out by Ghods et al. (2015), focusing on σ_1, σ_2 and σ_3. The outcome of the investigation demonstrated that the estimated values were 105/00, 270/90 and 15/00, respectively. In accordance with the methodology of Nouri et al. (2023), earthquake focal mechanisms were employed to deduce the spatially varying crustal stress. By means of this approach, trend and plunge values for the northwestern regions of Iran were computed, yielding 191/05 for σ_1, 330/83 for σ_2, and 101/04 for σ_3, respectively. Furthermore, a shape ratio of 0.37 was determined for the targeted area. Furthermore, previous investigations have been conducted utilizing earthquake focal mechanism data to explore the stress inversion technique, e.g. Zamani et al. (2008).

This study aims to examine the stress state induced by plate convergence and analyze the distribution of stress in the northeastern region of Iran. The aim of this research is to examine the stress regimes present in the North Tabriz Fault of Iran through stress inversion of earthquake focal mechanisms. The present study employs the repeated inversion method of focal mechanisms of earthquakes (Vavryčuk, 2014) to establish the values and directions of stress. This method is considered the most appropriate for the inversion of focal mechanisms, particularly when the nodal plane is unknown. The auxiliary nodal plane plays a crucial role in resolving the linear inversion problem (Michael, 1984). Furthermore, the independence of the central focal mechanisms and the error analysis have been accorded particular emphasis in the study.

2. Tectonic setting

The previous scientific inquiries into the global positioning system (GPS) have yielded a comprehensive examination of the distribution of deformation in Iran (Nilforoushan et al., 2003); Vernant et al., 2004; Bayer et al., 2006; Hessami et al., 2006; Walpersdorf et al., 2006; Masson et al., 2006, 2007; Tavakoli et al., 2008; Peyret et al., 2009; Djamour et al., 2010, 2011; Mousavi et al., 2013). The tectonic activity observed in the northwestern region of Iran is influenced by a range of factors. These factors are principally comprised of the

Archive of SID.ir

Archive of SID.ir

northward displacement of the Arabian indenter, the westward propulsion of the Anatolian plate along the North- and East-Anatolian faults, and the counter-directional tectonic movements and subduction taking place below the Greater Caucasus and the Apsheron–Balkhan sill, respectively, which are situated in the northward direction (McKenzie, 1972; Jackson, 1992; Copley and Jackson, 2006; Vernant and Chery, 2006; and Dabiri et al., 2011). The rate of convergence within the entire region is estimated to be approximately 20 $mm/year$, as reported by Vernant et al. (2004). The convergence movement causes a complicated system of reverse and strike-slip faults, which have been confirmed by GPS measurements. While the North Anatolian fault and other right-lateral faults in southeast Turkey seem to continue into the northwest region of Iran as strike-slip faults, as noted by Jackson (1992), there is no continuous faulting in both areas. Additionally, faulting in both regions comprises several distinct fault segments, according to the findings of Hessami et al. (2003b). The geographic region under investigation is situated within the longitude of 37 to 39 degrees east and the latitude of 45 to 47 degrees north, as illustrated in Figure 1. The North Tabriz Fault, which exhibits a minimum slip rate of 2 $mm/year$, a horizontal slip rate of 3.1 - 4 $mm/year$, and a vertical slip rate of 0.5 - 0.8 $mm/year$, has been responsible for past earthquakes in the region, some of which have caused significant surface rupture. Noteworthy examples include the Shibli (a village situated in the East Azerbaijan province near Tabriz, is positioned adjacent to the North Tabriz Fault) earthquake of 1721, with a magnitude of 7.3 and a surface rupture exceeding 35 km, and the Tabriz earthquake of 1780, with a magnitude of 7.4 and a surface rupture of more than 42 km, resulting in a separation of 2 to 4 meters (Berberian and Yeats, 1999).

3. Data

This study utilizes focal mechanism data from credible sources, including the Global Centered Moment Tensor (GCMT) from 2005 to 2022 and the Iranian Seismological Center (IRSC) from 2012 to 2019. The relevant data are presented in Table 1. The current investigation has employed focal mechanism information associated with seismic events exceeding a magnitude of 4 ($M_w \geq 4$). The studied area is shown in Figure 1. In this study, an iterative joint inversion method Vavryčuk (2014) is employed to determine the stress field in the northern fault region of Tabriz. In the North Tabriz Fault (NTF) area, the focal mechanism data and the GPS velocity field in the Eurasian fixed reference frame are illustrated in Figure 2. The GPS velocity field, which reflects the tectonic deformation and displacements in the northwestern region of Iran and around the NTF, was obtained from Khorrami et al. (2019).

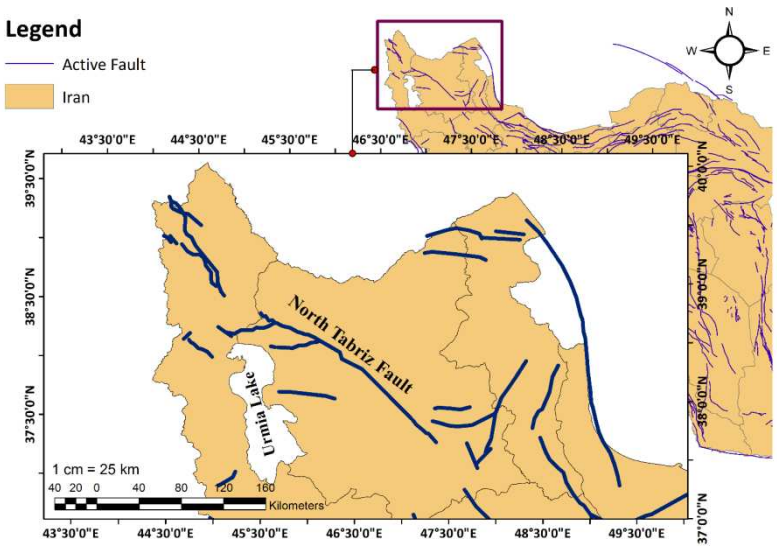

Figure 1. The present study focuses on the region encompassing the North Tabriz Fault (NTF) or the northwestern region of Iran, as illustrated by the demarcation of the North Tabriz Fault in the accompanying figure. The study area has been demarcated based on the set scale for this research. Fault tracing data is extracted from Hessami et al. (2003a).

Archive of SID.ir

Archive of SID.ir

Table 1. This table presents the data gathered from two reputable sources, namely GCMT and IRSC. The data pertains to the region situated in North Tabriz Fault and northwestern Iran and covers the latitude range of 37° to 39° and longitude range of 45° to 47°.

Number	Origin Time and Location Parameters						Nodal Plane 1			Nodal Plane 2			reference
	Date	Time	Latitude (°N)	Longitude (°E)	Depth (Km)	M w	strik e (°)	dip (°)	rake (°)	strike (°)	dip (°)	rake (°)	
1	20050926	18:57:11.9	37.36	47.77	19.8	5.2	194	43	55	57	56	118	CMT
2	20080902	20: 0:54.5	38.69	45.79	15.4	5.0	113	80	-179	23	89	-10	CMT
3	20120811	12:23:15	38.393	46.806	9.0	6.5	267	81	-175	176	85	-9	IRSC
4	20120811	12:23:20.9	38.31	46.80	15.0	6.5	175	81	6	84	84	170	CMT
5	20120811	12:34:34	38.394	46.814	4.0	6.3	7	57	21	265	72	146	IRSC
6	20120811	12:34:39.5	38.35	46.78	19.2	6.4	10	50	36	255	63	134	CMT
7	20120811	15:21:14	38.427	46.800	4.0	4.8	266	79	174	357	84	11	IRSC
8	20120811	15:43:19	38.461	46.737	7.4	4.9	35	57	67	253	39	121	IRSC
9	20120811	22:24: 6.1	38.35	46.73	27.4	5.2	345	59	1	254	89	149	CMT
10	20120811	22:24:02	38.434	46.752	4.0	5.2	82	89	-165	352	75	-1	IRSC
11	20120813	1:56:10	38.418	46.692	4.0	4.7	261	80	178	352	88	10	IRSC
12	20120814	14:02:25	38.503	46.810	7.4	5.1	92	83	-176	1	86	-7	IRSC
13	20120815	17:49:04	38.440	46.670	4.0	4.9	80	70	165	175	76	20	IRSC
14	20120815	17:49:08.8	38.39	46.71	13.2	5.0	246	50	133	10	56	51	CMT
15	20120816	17:14:14	38.540	46.770	10.0	4.8	256	84	165	348	76	6	IRSC
16	20120816	17:14:17.8	38.35	46.81	25.2	4.8	263	78	172	355	82	12	CMT
17	20121107	6:26:31	38.458	46.565	10.0	5.7	272	75	-173	181	84	-15	IRSC
18	20121107	06:26:33.3	38.40	46.61	15.0	5.6	183	83	7	92	83	173	CMT
19	20121116	3:58:25	38.480	46.570	10.0	4.8	195	67	1	104	89	157	IRSC
20	20121116	03:58:28.4	38.49	46.66	15.8	4.8	109	81	179	199	89	9	CMT
21	20121223	6:38:57	38.487	44.934	12.0	5.0	70	68	149	172	62	25	IRSC
22	20130126	15:10:49	38.361	46.837	6.0	4.9	9	72	37	267	55	158	IRSC
23	20130126	15:10:52.8	38.37	46.87	21.6	4.8	269	66	163	6	74	25	CMT
24	20130418	10:39:37	38.430	45.360	6.0	4.9	204	83	28	110	62	172	IRSC
25	20130418	10:39:41.5	38.38	45.39	20.4	4.9	114	61	155	217	68	32	CMT
26	20130927	10:02:43	37.330	44.940	7.0	4.5	196	43	16	94	79	132	IRSC
27	20131108	10:12:34	37.800	47.170	9.0	4.4	311	79	-173	220	83	-11	IRSC
28	20160622	16:56:58	38.50	44.86	4.0	4.3	304	88	-166	214	76	-2	IRSC
29	20170827	23:14:52.6	37.87	47.14	17.5	5.0	116	72	-177	26	87	-18	CMT
30	20191107	22:47:05	37.71	47.52	8.0	5.9	307	86	-164	216	74	-4	IRSC
31	20191108	13:51:45	37.74	47.40	8.0	4.5	109	78	-161	15	72	-13	IRSC
32	20191110	2:13:45	37.67	47.47	7.0	4.4	81	54	102	241	37	74	IRSC
33	20220921	17:57:58.2	38.41	45.09	21.2	5.0	309	53	173	43	84	38	CMT
34	20221005	0:21:32.4	38.41	45.11	26.2	5.7	299	63	174	31	84	27	CMT
35	20221005	13:51:42.9	38.43	45.17	33.0	4.8	200	82	-1	290	89	-172	CMT

Archive of SID.ir

Archive of SID.ir

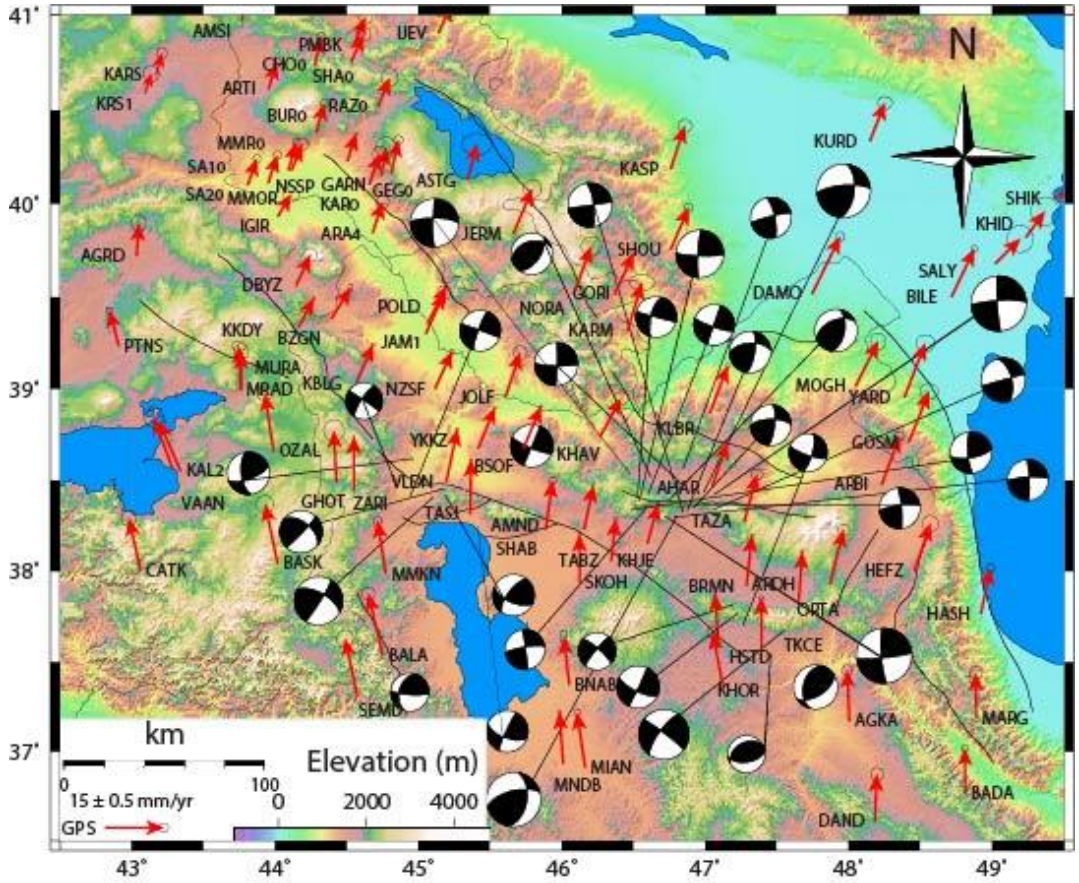

Figure 2. Tectonic map of active faults in the northwestern region of Iran. The red arrows signify the GPS velocity vectors that represent the region's tectonic deformation. The GPS velocity field data utilized in this figure was obtained from Khorrami et al. (2019), while the earthquake focal mechanism data were extracted from the trustworthy websites, namely Global Centroid Moment Tensor (GCMT) and Iranian Seismological Center (IRSC). The fault lines in the figure are identified by black lines and were obtained from Ambraseys and Melville (2005), Berberian and Yeats (1999) and Berberian (1994).

4. Methodology

4.1. Inversion for stress

The proposition of a technique for reversing the solution of the earthquake focal plane in order to deduce the orientation of the principal stresses was first presented by Angelier (1979). Determining the stress tensor in the crust cannot be accurately accomplished by relying on the focal mechanism of a single earthquake. To address this issue, an inversion algorithm is indispensable for obtaining the stress tensor via a substantial number of earthquakes, as stated by McKenzie (1969).

The problem of slip on a fault within a stress field was initially presented by Wallace (1951) and Bott (1959). In 1959, Bott put forth the notion that slip transpires on any fault plane in correspondence with the maximum shear stress achieved. Furthermore, it was demonstrated that the orientation of the shear stress is dependent on the orientation of the fault plane in the stress field and the shape ratio (R), which is defined as follows:

$$R = \frac{\sigma_1 - \sigma_2}{\sigma_1 - \sigma_3} \quad (1)$$

Regarding (1), the principal stresses are σ_1, σ_2 and σ_3, and consistently $\sigma_3 \leq \sigma_2 \leq \sigma_1$. Carey (1974) employed Bott's criterion for stress inversion and appended the postulate that the movements associated with all strike-slip faults result from a shared tensor.

4.2. Iterative joint inversion

The fault instability condition, initially introduced in Gephart and Forsyth's (1984) stress inversion method, was employed by Lund and Slunga (1999) to enhance its effectiveness. Subsequently, in Vavryčuk's (2014) iterative joint inversion technique, the same condition was implemented in Michael's (1984) approach.

According to Michael's (1984) linear inversion method, the principal stress direction can be determined with precision.

Archive of SID.ir

Archive of SID.ir

However, the R ratio estimation is associated with a substantial degree of error. In contrast to Gephart and Forsyth's (1984) method, Michael's method is linear in nature and demands resolution of stress reversal through multiple iterations, once the fault instability condition is imposed.

The approach employed by Michael (1984) involves utilizing the shear tension (τ) and normal tension (σ_n) exerted on the fault in the following manner:

$$\sigma_n = \mathrm{T}_i n_i = \tau_{ij} n_i n_j \quad (2)$$

$$\tau N_i = T_i\text{-}\sigma_n n_i = \tau_{ij} n_j - \tau_{jk} n_j n_k n_i = \tau_{kj} n_j (\delta_{ik} - n_i n_k) \quad (3)$$

where δ_{ik} the Kronecker's delta operator, T denotes the tension exerted along the fault, n signifies the normal vector of the fault, and N represents the direction of the shear stress unit vector along the fault. Equation (3) can be rewritten as follows:

$$\tau_{kj} n_j (\delta_{ik} - n_i n_k) = \tau N_i \quad (4)$$

In order to derive the right-hand side of Equation (3), Michael (1984) utilized the Wallace (1951) assumption to ascertain the orientation of shear stress and slip direction along the fault. Additionally, it was postulated that the magnitude of shear stress on the faults remained constant for all analyzed earthquakes. Due to the inability of this approach to determine the absolute stress value, the variable τ was normalized to 1 in Equation (4). Consequently, it was possible to represent Equation (4) as a matrix as follows:

$$At = s \quad (5)$$

where t is the vector of stress components.

$$t = [\tau_{11}\ \tau_{12}\ \tau_{13}\ \tau_{22}\ \tau_{23}] \quad (6)$$

and A is a matrix in terms of the normal vector n:

$$A = \begin{bmatrix} n_1(n_2^2 + 2n_2^2) & n_2(1 - 2n_1^2) & n_3(1 - 2n_1^2) & n_1(-n_2^2 + n_3^2) & -2n_1 n_2 n_3 \\ n_2(-n_1^2 + n_3^2) & n_1(1 - 2n_2^2) & -2n_1 n_2 n_3 & n_2(n_1^2 + 2n_3^2) & n_3(1 - 2n_2^2) \\ n_3(-2n_1^2 - n_2^2) & -2n_1 n_2 n_3 & n_1(1 - 2n_3^2) & n_3(-n_1^2 - 2n_2^2) & n_2(1 - 2n_3^2) \end{bmatrix} \quad (7)$$

Furthermore, the slip vector's orientation is represented by the symbol s. The focal mechanisms of Equation (7) is utilized to determine the stress tensor's five unknown components by incorporating the slip direction and normal vector of k earthquakes and generating $3k$ linear equations. The generalized linear inversion technique (Lay and Wallace, 1995) is employed to solve the system of equations by inserting it into Equation (2).

$$t = \mathrm{A}^{-1} s \quad (8)$$

The vector s is obtained from Equations (9) to (11) as follows:

$$s_1 = \cos(rake) \times \cos(strike) + \cos(dip) \times \sin(rake) \times \sin(strike) \quad (9)$$

$$s_2 = \cos(rake) \times \sin(strike) - \cos(dip) \times \sin(rake) \times \cos(strike) \quad (10)$$

$$s_3 = -\sin(rake) \times \sin(dip) \quad (11)$$

Also, the components of the vector n can be written as follows:

$$n_1 = -\sin(dip) \times \sin(strike) \quad (12)$$

$$n_2 = \sin(dip) \times \cos(strike) \quad (13)$$

$$n_3 = -\cos(dip) \quad (14)$$

To ascertain the optimal deviatoric stress tensor, it is essential to evaluate two measures. The first quantity, referred to as β, establishes the degree of orientation between the predicted tangential tension and the fault plane slip direction on each plane, as depicted in Figure 3. An ideal scenario is when this angle is zero; however, this is not always feasible. The second measure is the magnitude of τ or $\vec{\tau}$, which should ideally be one, yet this is not always the case.

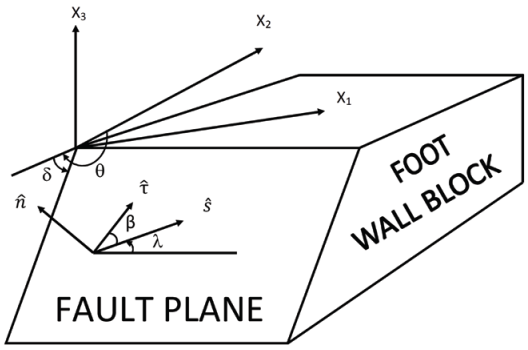

Figure 3. displays a schematic representation of the foot wall block. The symbols θ, δ and λ correspond to the strike, the dip and the rake, respectively. Additionally, $\hat{n}$ and $\hat{s}$ signify the outward normal to the foot wall block and the slip vector within the fault plane, respectively. The parameter β refers to the angle between $\hat{s}$ and $\hat{\tau}$, which represents the tangential traction predicted by a stress tensor (Michael, 1984).

The linear inversion technique aims to reduce

Archive of SID.ir

Archive of SID.ir

the discrepancy between the calculated shear stress vector and the observed slip vector.

As a generalization, the slip plane is anticipated to exhibit greater instability. Moreover, it is feasible to discern the plane in closest proximity to Mohr's envelope based on the stress diagram of Mohr's circle (Jaeger et al., 2009). The Relative magnitude of the principal stresses (R) is adequate to generate a Mohr's circle in three dimensions, with no requirement of a scale, as stated by Gephart and Forsyth (1984). The spatial arrangement of the nodal planes in relation to the principal stress field determines their location on the Mohr diagram. By utilizing the Mohr diagram derived from the four tensor components produced from the earthquake focal mechanism inversion process, for all sliding friction coefficients, it is possible to detect the nodal plane possessing the greatest instability. According to Vavryčuk et al. (2013), the instability relationship used in the iterative joint inversion method from the focal mechanism of earthquakes can be expressed as follows:

$$I = \frac{\tau - \mu(\sigma - 1)}{\mu + \sqrt{1+\mu^2}} \quad (15)$$

where:

$$\sigma = n_1^2 + (1-2R)n_2^2 - n_3^2 \quad (16)$$

$$\tau = \sqrt{n_1^2 + (1-2R)^2 n_2^2 + n_3^2 - [n_1^2 + (1-2R)^2 n_2^2 + n_3^2]^2} \quad (17)$$

The degree of instability is expressed as a numerical value between zero, indicating the highest degree of stability, and one, indicating the lowest degree of stability.

The iterative joint inversion method to determine the focal mechanisms of earthquakes involves the initial utilization of Michael's method in a standard manner, devoid of any preconditions or knowledge of the fault plates' orientation. The principal stress direction and R ratio are then obtained, and their values are subsequently employed to evaluate the instability (as per Equation (15)) of the nodal plane for all the inverted focal mechanisms. The nodal planes that exhibit the highest level of instability are those of the fault planes.

The initial fault plane orientations acquired from the first iteration are utilized in the subsequent iteration via Michael's method. This process is subsequently iterated until the stresses reach an optimum value.

Following the completion of six repetitions in the present study, the stresses reached their optimal value. In order to assess the instability of faults using Equation (15), it is imperative to possess a friction coefficient value μ. The friction coefficient within the fault region generally varies between 0.2 and 0.8, but the specific value for the North Tabriz fault remains unknown. In the inversion process, it is common to assign an average value, such as 0.6, to the friction coefficient. Alternatively, the inversion can be conducted using multiple values, and the value that yields the highest instability can estimate the optimal friction coefficient for the region. Vavryčuk (2014) conducted numerical tests that demonstrate the iterative joint inversion method for stress to be rapid, precise and superior to the conventional linear inversion method.

4.3. Maximum horizontal stress orientation (SH)

In the event that all six constituents of the stress tensor have been ascertained, it is possible to calculate the magnitude and orientation of the maximum horizontal stress (SH). Alternatively, if only four components of the stress tensor are accessible, namely σ_1, σ_2, σ_3 and R, then the direction of SH can be inferred Lund and Townend (2007). For the purposes of this investigation, the principal stress directions and shape ratio (R) have been determined through the iterative joint inversion method. Consequently, the approach outlined by Lund and Townend (2007) can be employed to determine the direction of SH.

In this study, there are two distinct systems of coordinates that warrant attention: the first is the coordinate system of principal stress (S), which comprises unit vectors ($\hat{s}_1$, $\hat{s}_2$, $\hat{s}_3$) aligned with the maximum, intermediate and minimum principal stresses. The second system is the geographic coordinate system (G), which consists of unit vectors ($\hat{g}_1$, $\hat{g}_2$, $\hat{g}_3$) oriented towards the north, east and down.

The expression of the transfer matrix between S and G coordinate systems is presented as follows:

Archive of SID.ir

Archive of SID.ir

$$A_{SG} = \begin{bmatrix} \hat{s}_1\hat{g}_1 & \hat{s}_1\hat{g}_2 & \hat{s}_1\hat{g}_3 \\ \hat{s}_2\hat{g}_1 & \hat{s}_2\hat{g}_2 & \hat{s}_2\hat{g}_3 \\ \hat{s}_3\hat{g}_1 & \hat{s}_3\hat{g}_2 & \hat{s}_3\hat{g}_3 \end{bmatrix} \quad (18)$$

Consequently, as per the transfer matrix, the normal vector in the principal stress coordinate system shall be as follows:

$$\hat{n}_s = A_{SG}\hat{n}_G = \begin{bmatrix} s_{1N}n_N + s_{1E}n_E \\ s_{2N}n_N + s_{2E}n_E \\ s_{3N}n_N + s_{3E}n_E \end{bmatrix} \quad (19)$$

where, for example, s_{1N} is the northern component of the vector $\hat{s}_1$.

The definition of a vertical plane within the geographic coordinate system is established through its normal vectors:

$$\hat{n}_G^T = (n_N, n_E, n_D) = (cos\alpha, sin\alpha, 0) \quad (20)$$

where α refers to the angle formed between the normal vector of the vertical plane and the north direction in a clockwise manner. As a result, the vertical plane's extension is equivalent to $\alpha + \frac{\pi}{2}$.

The stress tensor takes on a diagonal matrix form when expressed within the principal stress coordinate system:

$$S = \begin{bmatrix} \sigma_1 & 0 & 0 \\ 0 & \sigma_2 & 0 \\ 0 & 0 & \sigma_3 \end{bmatrix} \quad (21)$$

To evaluate the orientation of the maximum horizontal stress (SH), the stress tensor (S) is partitioned into two components, namely deviant (D) and isotropic $(\sigma_3 I)$ parts, in the principal stress coordinate system:

$$S = (\sigma_1 - \sigma_1)\begin{bmatrix} 1 & 0 & 0 \\ 0 & 1-R & 0 \\ 0 & 0 & 0 \end{bmatrix} + \sigma_3 I \quad (22)$$

The process of obtaining the deviatoric normal stress vector $(\hat{d}_n)$ involves transferring a normal vertical plane from the geographic coordinate system $(\hat{n}_G)$ to the principal stress coordinate system using a transfer matrix to obtain $\hat{n}_s$. In the determination of the normal stress components on the vertical plane, consideration is only given to the SH direction, while the isotropic part of the stress tensor is disregarded, since it plays no role in determining the direction of SH. Accordingly, the deflection component of the normal stress on the vertical plane is expressed as:

$$\hat{d}_n = (\hat{n}_s^T D\hat{n}_s)\hat{n}_s = (\sigma_1 - \sigma_3)[(s_{1N}n_N + s_{1E}n_E)^2 + (1-R)(s_{2N}n_N + s_{2E}n_E)^2]\hat{n}_s = D_n\hat{n}_s \quad (23)$$

where $\hat{d}_n$ is the horizontal deviatoric stress in the direction α.

The orientation of SH is obtained through the derivation of the magnitude of vector $(D_n)\hat{d}_n$.

$$\frac{dD_n}{d\alpha} = (\sigma_1 - \sigma_3)[(s_{1E}^2 - s_{1N}^2) + (1-R)(s_{2E}^2 - s_{2N}^2)]sin2\alpha + 2(\sigma_1 - \sigma_3)[s_{1N}s_{1E} + (1-R)s_{2N}s_{2E}]cos2\alpha \quad (24)$$

Through the process of equating the derivative to zero, it is possible to determine the points at which d_n attains its maximum and minimum values:

$$tan2\alpha = \frac{2(s_{1N}s_{1E} + (1-R)s_{2N}s_{2E})}{(s_{1N}^2 - s_{1E}^2) + (1-R)(s_{2N}^2 - s_{2E}^2)} \quad (25)$$

5. Results

The present research work has determined that the optimal friction coefficient for the North Tabriz fault is 0.6. Furthermore, the shape ratio value was found to be nearly high, approximately equal to 0.95. The Plunge value for σ_1 and σ_3 was observed to be relatively negligible and amounted to 3.24 and 2.06, respectively. A value of nearly 90 degrees was estimated for σ_2, which equates to 86.14. The trend values for σ_1 and σ_3 were found to be 146.08 and 55.97, respectively, while the same value of 293.51 was obtained for σ_2. The iterative joint inversion method was utilized to estimate the orientation of the maximum horizontal stress (SH), resulting in an estimation of $\alpha = 3.787°$. The trend and plunge obtained from this method for σ_1, σ_2 and σ_3 were also utilized for this estimation.

By utilizing the earthquake focal mechanisms enumerated in Table 1, we analyze the state of the prevailing stress field and the orientation of the maximum horizontal stress (SH) in the region marked in Figure 1. To conduct the stress inversion using focal mechanisms of earthquakes, it is necessary to differentiate the principal fault plane from the auxiliary plane. Failure to obtain this information and align the nodal planes can lead to inaccurate results. Michael's linear inversion method does not offer the option of selecting fault planes, but is effective in identifying the principal stress direction. The

Archive of SID.ir

Archive of SID.ir

findings of the inversion performed through Michael's linear method are presented in Table 2. Table 3 demonstrates the outcomes of the iterative joint inversion method utilized for the North Tabriz fault zone.

Figure 4 presents the outcomes obtained through the iterative joint inversion technique, encompassing the orientation of the principal stress and the maximum horizontal stress orientation (SH).

The principal stress axes within the NTF region are depicted in Figure 5 and the Bar graph of the region's shape ratio can be observed in Figure 6. The sensitivity of the shape ratio relies heavily on the accurate selection of faults, with the substitution of faults by auxiliary nodal planes leading to notable errors. Through conducting numerical tests, we demonstrate the remarkable robustness of the iterative joint inversion method in determining stress and fault orientations, resulting in significantly improved accuracy in calculating the shape ratio. The levels of uncertainty pertaining to the principal stresses calculations are displayed in Figure 7.

Table 2. The results of inversion by Michael's linear method.

$\sigma_1(°)$		$\sigma_2(°)$		$\sigma_3(°)$		Shape Ratio
Trend	Plunge	Trend	Plunge	Trend	Plunge	0.8629
-34.6438	2.7374	-165.6016	85.8282	55.5068	3.1457	

Table 3. The results of iterative joint inversion method.

$\sigma_1(°)$		$\sigma_2(°)$		$\sigma_3(°)$		Shape Ratio
Trend	Plunge	Trend	Plunge	Trend	Plunge	0.9529
146.0894	3.2476	293.5134	86.1478	55.9719	2.0697	

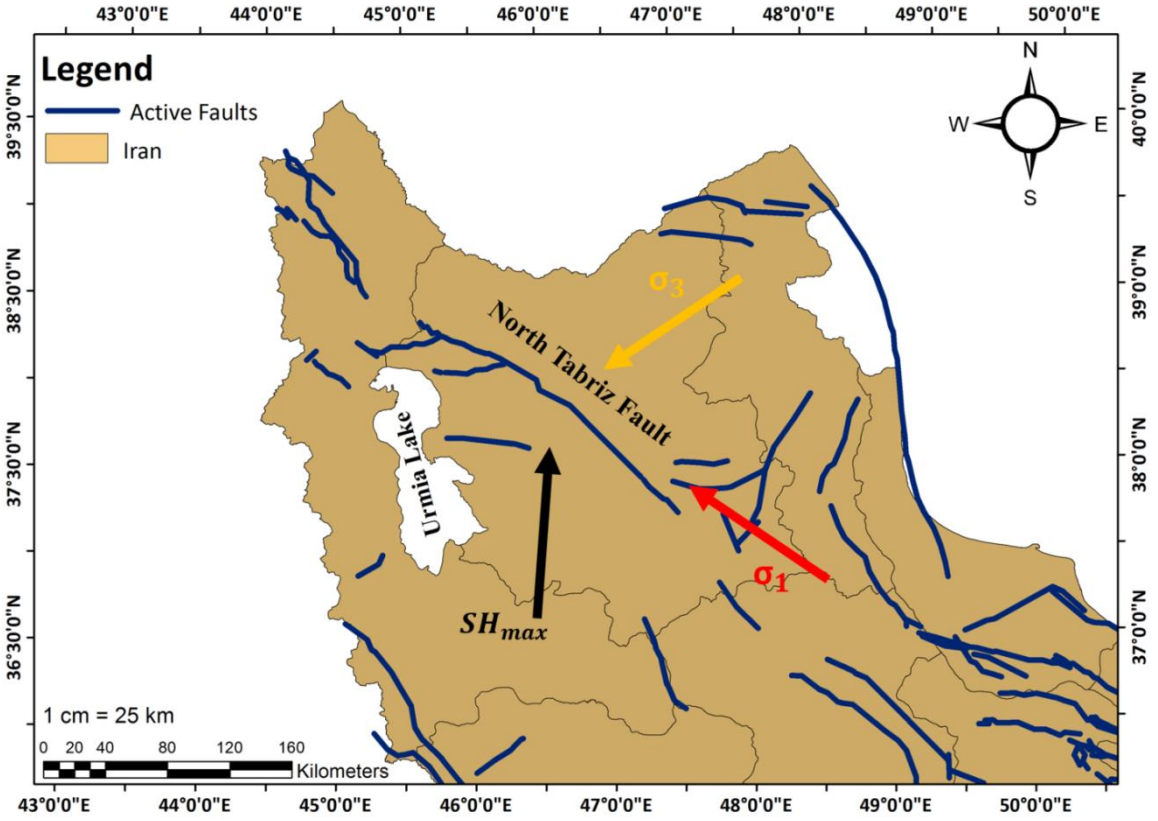

Figure 4 The results of the iterative joint inversion method for the direction of the principal stresses and the maximum horizontal stress orientation (SH). Fault tracing data is extracted from Hessami et al. (2003a).

Archive of SID.ir

Archive of SID.ir

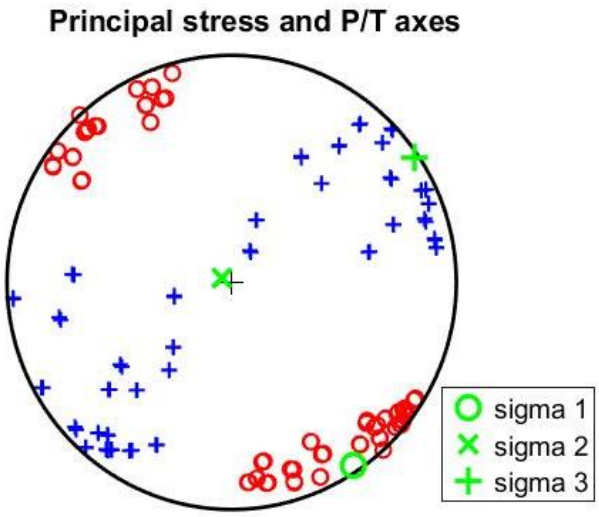

Figure 5. The principal stresses in the North Tabriz Fault. The circles within the figure correspond to values of σ_1, the multiplication sign denotes σ_2, and the plus sign represents σ_3 for each occurrence. The derivations of these stresses are indicated by the green color.

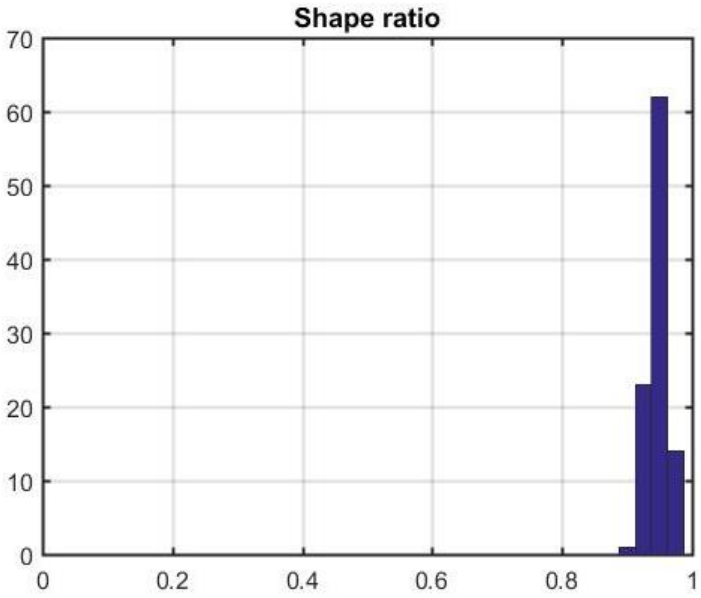

Figure 6. The Bar graph of the shape ratio.

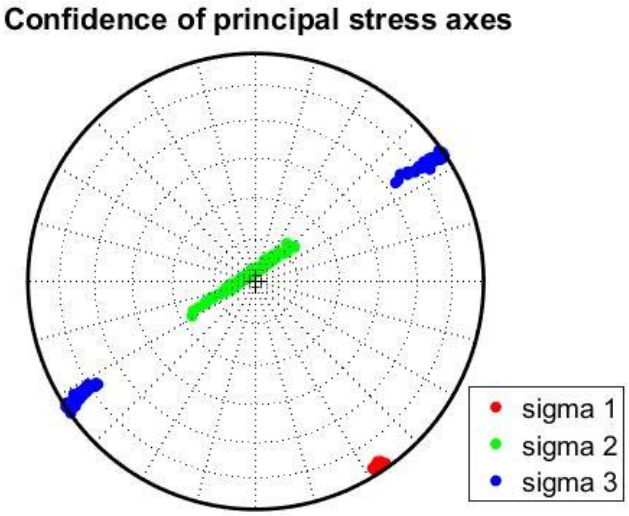

Figure 7. This figure presents the levels of uncertainty in the determination of principal stresses. The confidence levels for σ_1, σ_2 and σ_3 axes are depicted by the colors red, green and blue, respectively.

Archive of SID.ir

Archive of SID.ir

The graphical technique known as Mohr's Circle is utilized for the determination of stress on a given plane within a stressed structure. Moreover, Mohr's Circle can be employed for the three-dimensional depiction of stress. Figure 8 depicts the Mohr's circle diagram utilizing Vavryčuk's (2014) method for the data analyzed in this investigation within the North Tabriz fault zone. The construction of a Mohr pie chart illustrates that the faults identified through the inversion process exhibit a prevalence of upper fault instability, primarily concentrated within the region of validity defined by the Mohr-Coulomb failure criterion. This noteworthy observation serves as compelling evidence for the consistency between the data and the fault instability model, validating the suitability of the iterative joint stress inversion technique. Conversely, in cases where the faults identified by the inversion do not exhibit significant instability, it is likely that the fault instability model may not be entirely appropriate, thereby resulting in potentially less reliable outcomes from the iterative inversion methodology.

6. Discussion

In this study, the focal mechanisms of earthquakes in the vicinity of the NTF fault system were inverted using the iterative joint inversion method to determine the orientation of principal stresses and orientation of the maximum horizontal stress (SH). An error analysis was conducted to ensure the accuracy of the results. The findings indicate that the iterative joint inversion method yields highly precise and reliable data, with a low error rate and uncertainty as shown in Figure 7. The calculated principal stresses exhibited minimal errors (maximum 5.933), underscoring the suitability of the iterative joint inversion method as a means to invert focal mechanisms for stress field identification, even in cases where the main nodal plane is unknown from the auxiliary nodal plane. Moreover, the results of this study are consistent with the stress studies conducted by Afra et al. (2017), Ghods et al. (2015), Nouri et al. (2023) and Karakhanian et al. (2004).

The stress axes derived from the inversion (as shown in Figure 5) suggest that σ_1 is oriented in a southeast-northwest direction, which corresponds well with the movement of the Arabian plate towards the Eurasian plate. The area under investigation in this study exhibits a considerable shape ratio, indicating either a significant dissimilarity between the maximum and average principal stress or a minor difference between the maximum and minimum principal stress.

The prevailing stress orientation within the investigated region signifies a prevalence of strike-slip faults adjacent to the NTF fault system. The stress direction that was detected in this inquiry (~3°) and the trend of the NTF fault system (~146°) point towards the likelihood of a transpressional mechanism governing the NTF.

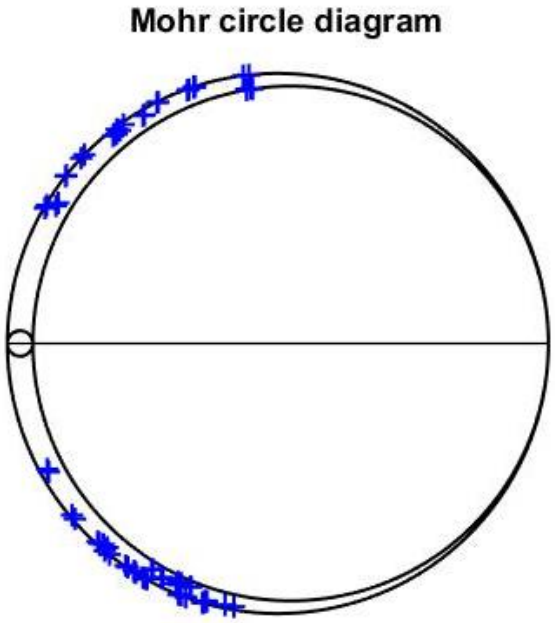

Figure 8. Mohr's circle diagram for the data analyzed in this study.

Archive of SID.ir

Archive of SID.ir

In this study, the analysis of calculation errors was conducted using two methods, namely Michael's method and the iterative joint inversion method for stress axes and shape ratio, in the area under investigation. The results demonstrated that the iterative joint inversion method exhibited superiority in identifying the stress field due to their lower error rate (maximum error of 1.9 as compared to 23.85 in Michael's linear method). An examination of the strike, dip and rake variables in the inversion analysis revealed that alterations made to the dip value have a noteworthy effect on identifying the optimal location of horizontal stress.

As per Anderson (1905) and Célérier (2008) study as well as the Anderson's theory of faulting, when it comes to faults and strike-slip occurrences, the plunge readings for σ_1 and σ_3 are anticipated to be in proximity to zero, and the plunge value for σ_2 is projected to be about 90, which corresponds with the findings of this investigation.

7. Conclusion

To understand the deformation of geological structures, movements of plates, and mechanics of tectonics, it is essential to possess the knowledge of stress states. The objective of this research was to investigate stress regimes in the North Tabriz Fault and the northwestern Iran region as a whole. To accomplish this objective, a stress inversion of 35 compiled focal mechanisms was performed to establish the orientation of principal stress axes and stress ratio. The results of our analysis of the earthquake focal mechanisms were indicative of right-lateral strike-slip motion, thereby corroborating the dominant tectonics in the region.

The findings validates the presence of strike-slip movements in the northwestern region of Iran and the North Tabriz Fault, which aligns with similar investigations conducted in the area by McKenzie (1972) and Karakhanian et al. (2004). Despite the recent stress mapping efforts by Zarifi et al. (2014) that indicate northwestern Iran's NW shortening, this seismic examination reveals considerable heterogeneity in the area, with east-west contraction being the dominant feature.

The present study revealed that the prevailing stress, determined via the iterative joint inversion method, conforms to the stress contour depicted on the world stress map. Additionally, the error assessment indicates that the iterative joint inversion method outperforms Michael's method in identifying the stress field.

Acknowledgements

All authors contributed to the study conception and design. Material preparation, data collection and analysis were performed by Milad Salmanian, Asghar Rastbood and Masoud Mashhadi Hossainali. The first draft of the manuscript was written by Milad Salmanian and all authors commented on previous versions of the manuscript. All authors read and approved the final manuscript. The authors did not receive support from any organization for the submitted work.

Declaration of competing interest

There is no conflict of interest to declare.

References

Aflaki, M., Shabanian, E., Sahami, S., & Arshadi, M. (2021). Evolution of the stress field at the junction of Talesh–Alborz–Central Iran during the past 5 Ma: implications for the tectonics of NW Iran. *Tectonophysics*, 821, 229115.

Afra, M., Moradi, A., & Pakzad, M. (2017). Stress regimes in the northwest of Iran from stress inversion of earthquake focal mechanisms. *Journal of Geodynamics*, 111, 50-60.

Agard, P., Omrani, J., Jolivet, L., Whitechurch, H., Vrielynck, B., Spakman, W., Monié, P., Meyer, B., & Wortel, R. (2011). Zagros orogeny: a subduction-dominated process. *Geological Magazine*, 148(5-6). 692-725.

Allen, M., Jackson, J., & Walker, R. (2004). Late Cenozoic reorganization of the Arabia-Eurasia collision and the comparison of short-term and long-term deformation rates. *Tectonics*, 23(2).

Ambraseys, N. N., & Melville, C. P. (2005). A history of Persian earthquakes, Cambridge university press.

Anderson, E. M. (1905). The dynamics of faulting. *Transactions of the Edinburgh Geological Society*, 8(3). 387-402.

Angelier, J. (1979). Determination of the mean principal directions of stresses for a given fault population. *Tectonophysics*, 56(3-4), T17-T26.

Archive of SID.ir

Archive of SID.ir

Arnold, R., & Townend, J. (2007). A Bayesian approach to estimating tectonic stress from seismological data. *Geophysical Journal International*, 170(3), 1336-1356.

Bayer, R., Chery, J., Tatar, M., Vernant, P., Abbassi, M., Masson, F., Nilforoushan, F., Doerflinger, E., Regard, V., & Bellier, O. (2006). Active deformation in Zagros—Makran transition zone inferred from GPS measurements. *Geophysical Journal International*, 165(1), 373-381.

Berberian, M. (1994). Natural hazards and the first earthquake catalogue of Iran: historical hazards in Iran prior to 1900, UNESCO.

Berberian, M., & Yeats, R. S. (1999). Patterns of historical earthquake rupture in the Iranian Plateau. *Bulletin of the Seismological society of America*, 89(1), 120-139.

Bott, M. H. P. (1959). The mechanics of oblique slip faulting. *Geological magazine*, 96(2), 109-117.

Carey, E. (1974). Analyse theorique et rumerique d'un modele mecanique elementaire applique a l'etude d'une population de failles: Comptes Rendus Hebdomadaires des Seances de l'Academie des Sciences, Serie D, *Sciences Naturelles*, 279(11), 891-894.

Célérier, B. (2008). Seeking Anderson's faulting in seismicity: a centennial celebration. *Reviews of Geophysics*, 46(4).

Copley, A., & Jackson, J. (2006). Active tectonics of the Turkish-Iranian plateau. *Tectonics*, 25(6).

Dabiri, R., Emami, M., Mollaei, H., Chen, B., Abedini, M., Omran, N., & Ghaffari, M. (2011). Quaternary post-collision alkaline volcanism NW of Ahar (NW Iran): geochemical constraints of fractional crystallization process. *Geologica Carpathica*, 62(6), 547.

Dewey, J., Hempton, M., Kidd, W., Saroglu, F., & Şengör, A. (1986). Shortening of continental lithosphere: the neotectonics of Eastern Anatolia—a young collision zone. *Geological Society, London, Special Publications*, v. 19, no. 1, p. 1-36.

Djamour, Y., Vernant, P., Bayer, R., Nankali, H. R., Ritz, J.-F., Hinderer, J., Hatam, Y., Luck, B., Le Moigne, N., & Sedighi, M. (2010). GPS and gravity constraints on continental deformation in the Alborz mountain range, Iran. *Geophysical Journal International*, 183(3), 1287-1301.

Djamour, Y., Vernant, P., Nankali, H. R., & Tavakoli, F. (2011). NW Iran-eastern Turkey present-day kinematics: results from the Iranian permanent GPS network. *Earth and Planetary Science Letters*, 307(1-2), 27-34.

Gephart, J. W., & Forsyth, D. W. (1984). An improved method for determining the regional stress tensor using earthquake focal mechanism data: application to the San Fernando earthquake sequence, *Journal of Geophysical Research: Solid Earth*, 89(B11), 9305-9320.

Ghods, A., Shabanian, E., Bergman, E., Faridi, M., Donner, S., Mortezanejad, G., & Aziz-Zanjani, A. (2015). The Varzaghan–Ahar, Iran, Earthquake Doublet (M w 6.4, 6.2): implications for the geodynamics of northwest Iran. *Geophysical Journal International*, 203(1), 522-540.

Hardebeck, J. L., & Michael, A. J. (2006). Damped regional-scale stress inversions: Methodology and examples for southern California and the Coalinga aftershock sequence. *Journal of Geophysical Research: Solid Earth*, 111(B11).

Hempton, M. R. (1987). Constraints on Arabian plate motion and extensional history of the Red Sea. *Tectonics*, 6(6), 687-705.

Hessami, K., Jamali, F., & Tabassi, H. (2003a). Major active faults of Iran. *IIEES*, Tehran.

Hessami, K., Nilforoushan, F., & Talbot, C. J. (2006). Active deformation within the Zagros Mountains deduced from GPS measurements. *Journal of the Geological Society*, 163(1), 143-148.

Hessami, K., Pantosti, D., Tabassi, H., Shabanian, E., Abbassi, M. R., Feghhi, K., & Solaymani, S. (2003b). Paleoearthquakes and slip rates of the North Tabriz Fault, NW Iran. *preliminary results: Annals of Geophysics*.

Jackson, J. (1992). Partitioning of strike-slip and convergent motion between Eurasia and Arabia in eastern Turkey and the Caucasus. *Journal of Geophysical Research: Solid Earth*, 97(B9), 12471-12479.

Jackson, J., & McKenzie, D. (1984). Active tectonics of the Alpine—Himalayan Belt

Archive of SID.ir

Archive of SID.ir

between western Turkey and Pakistan. *Geophysical Journal International*, 77(1), 185-264.

Jacques, A. (2002). Inversion of earthquake focal mechanisms to obtain the seismotectonic stress IV—a new method free of choice among nodal planes. *Geophysical Journal International*, 150(3), 588-609.

Jaeger, J. C., Cook, N. G., & Zimmerman, R. (2009). Fundamentals of rock mechanics, John Wiley & Sons.

Karakhanian, A. S., Trifonov, V. G., Philip, H., Avagyan, A., Hessami, K., Jamali, F., Bayraktutan, M. S., Bagdassarian, H., Arakelian, S., & Davtian, V. (2004). Active faulting and natural hazards in Armenia, eastern Turkey and northwestern Iran. *Tectonophysics*, 380(3-4), 189-219.

Khorrami, F., Vernant, P., Masson, F., Nilfouroushan, F., Mousavi, Z., Nankali, H., Saadat, S. A., Walpersdorf, A., Hosseini, S., & Tavakoli, P. (2019). An up-to-date crustal deformation map of Iran using integrated campaign-mode and permanent GPS velocities. *Geophysical Journal International*, 217(2), 832-843.

Lay, T., & Wallace, T. C. (1995). Modern global seismology, Elsevier.

Lund, B., & Slunga, R. (1999). Stress tensor inversion using detailed microearthquake information and stability constraints: Application to Ölfus in southwest Iceland. *Journal of Geophysical Research: Solid Earth*, 104(B7), 14947-14964.

Lund, B., & Townend, J. (2007). Calculating horizontal stress orientations with full or partial knowledge of the tectonic stress tensor. *Geophysical Journal International*, 170(3), 1328-1335.

Masson, F., Anvari, M., Djamour, Y., Walpersdorf, A., Tavakoli, F., Daignieres, M., Nankali, H., & Van Gorp, S. (2007). Large-scale velocity field and strain tensor in Iran inferred from GPS measurements: new insight for the present-day deformation pattern within NE Iran, *Geophysical Journal International*, 170(1), 436-440.

Masson, F., Djamour, Y., Van Gorp, S., Chéry, J., Tatar, M., Tavakoli, F., Nankali, H., & Vernant, P. (2006). Extension in NW Iran driven by the motion of the South Caspian Basin. *Earth and Planetary Science Letters*, 252(1-2), 180-188.

Maury, J., Cornet, F. H., & Dorbath, L. (2013). A review of methods for determining stress fields from earthquakes focal mechanisms; Application to the Sierentz 1980 seismic crisis (Upper Rhine graben). *Bulletin de la Societe Geologique de France*, 184(4-5), 319-334.

McKenzie, D. (1972). Active tectonics of the Mediterranean region. *Geophysical Journal International*, 30(2), 109-185.

McKenzie, D. P. (1969). The relation between fault plane solutions for earthquakes and the directions of the principal stresses. *Bulletin of the Seismological Society of America*, 59(2), 591-601.

Michael, A. J. (1984). Determination of stress from slip data: faults and folds. *Journal of Geophysical Research: Solid Earth*, 89(B13), 11517-11526.

Mousavi, Z., Walpersdorf, A., Walker, R., Tavakoli, F., Pathier, E., Nankali, H., Nilfouroushan, F., & Djamour, Y. (2013). Global Positioning System constraints on the active tectonics of NE Iran and the South Caspian region. *Earth and Planetary Science Letters*, 377, 287-298.

Mouthereau, F., Lacombe, O., & Vergés, J. (2012). Building the Zagros collisional orogen: timing, strain distribution and the dynamics of Arabia/Eurasia plate convergence. *Tectonophysics*, 532, 27-60.

Niassarifard, M., Shabanian, E., Azad, S. S., & Madanipour, S. (2021). New tectonic configuration in NW Iran: Intracontinental dextral shear between NW Iran and SE Anatolia. *Tectonophysics*, 811, 228886.

Nilforoushan, F., Masson, F., Vernant, P., Vigny, C., Martinod, J., Abbassi, M., Nankali, H., Hatzfeld, D., Bayer, R., & Tavakoli, F. (2003). GPS network monitors the Arabia-Eurasia collision deformation in Iran, *Journal of Geodesy*, 77, 411-422.

Nouri, A., Rahimi, B., Vavryčuk, V., & Ghaemi, F. (2023). Spatially varying crustal stress along the Zagros seismic belt inferred from earthquake focal mechanisms. *Tectonophysics*, 846, 229653.

Peyret, M., Djamour, Y., Hessami, K., Regard, V., Bellier, O., Vernant, P.,

Archive of SID.ir

Archive of SID.ir

Daignieres, M., Nankali, H., Van Gorp, S., & Goudarzi, M. (2009). Present-day strain distribution across the Minab-Zendan-Palami fault system from dense GPS transects. *Geophysical Journal International*, 179(2), 751-762.

Tavakoli, F., Walpersdorf, A., Authemayou, C., Nankali, H., Hatzfeld, D., Tatar, M., Djamour, Y., Nilforoushan, F., & Cotte, N. (2008). Distribution of the right-lateral strike–slip motion from the Main Recent Fault to the Kazerun Fault System (Zagros, Iran): Evidence from present-day GPS velocities. *Earth and Planetary Science Letters*, 275(3-4), 342-347.

Vavryčuk, V. (2014). Iterative joint inversion for stress and fault orientations from focal mechanisms. *Geophysical Journal International*, 199(1), 69-77.

Vavryčuk, V., Bouchaala, F., & Fischer, T. (2013). High-resolution fault image from accurate locations and focal mechanisms of the 2008 swarm earthquakes in West Bohemia, Czech Republic. *Tectonophysics*, 590, 189-195.

Vernant, P., & Chery, J. (2006). Low fault friction in Iran implies localized deformation for the Arabia–Eurasia collision zone. *Earth and Planetary Science Letters*, 246(3-4), 197-206.

Vernant, P., Nilforoushan, F., Hatzfeld, D., Abbassi, M., Vigny, C., Masson, F., Nankali, H., Martinod, J., Ashtiani, A., & Bayer, R. (2004). Present-day crustal deformation and plate kinematics in the Middle East constrained by GPS measurements in Iran and northern Oman. *Geophysical Journal International*, 157(1), 381-398.

Wallace, R. E. (1951). Geometry of shearing stress and relation to faulting. *The Journal of geology*, 59(2), 118-130.

Walpersdorf, A., Hatzfeld, D., Nankali, H., Tavakoli, F., Nilforoushan, F., Tatar, M., Vernant, P., Chéry, J., & Masson, F. (2006). Difference in the GPS deformation pattern of North and Central Zagros (Iran). *Geophysical Journal International*, 167(3), 1077-1088.

Zamani, B. (2013). Stress State Study of Siah Cheshmeh-Khoy Fault Zone (NW-Iran) and Using Stress Separation Method in Separation of Neotectonic Stresses from Paleostresses. *Scientific Quarterly Journal of Geosciences*, 23(89), 75-88. doi: 10.22071/gsj.2013.53557

Zamani, B., Angelier, J., & Zamani, A. (2008). State of stress induced by plate convergence and stress partitioning in northeastern Iran, as indicated by focal mechanisms of earthquakes. *Journal of Geodynamics*, 45(2-3), 120-132.

Zarifi, Z., Nilfouroushan, F., & Raeesi, M. (2014). Crustal stress map of Iran: insight from seismic and geodetic computations. *Pure and Applied Geophysics*, 171, 1219-1236.

Archive of SID.ir